Influence of Different Velocities on Muzzle Flow Field

LI Zijie, *WANG Hao**

School of Energy and Power Engineering, Nanjing University of Science and Technology, Nanjing 210094, P.R. China

(Received 9 October 2016; revised 5 September 2018; accepted 25 December 2018)

Abstract: A two-dimensional axisymmetric numerical simulation was successfully carried out on the muzzle flow field of a 300 mm-caliber counter-mass propelling gun. Based on the FLUENT software, using the finite volume method (FVM) and the realizable k-ε turbulence model, we adopted the holistic movement of a partitioned mesh processing method coupled with the intermediate ballistic model and the six degree-of-freedom model (6-DOF). We compared the flow field characteristics at the velocity of 1 730.4, 978.3, and 323.4 m/s. The results indicate that the pressure of the hypersonic initial flow field is much higher than that of the subsonic and supersonic initial flow fields. In the case of the subsonic (323.4 m/s) flow field, the tiny disturbance spreads throughout the whole domain. But in the cases of the supersonic (978.3 m/s) and the hypersonic (1 730.4 m/s) flow fields, it cannot spread to the upstream disturbance source, and the disturbance domain of the supersonic flow field is wider than that of the hypersonic. It is noted that the subsonic flow field has a rounded shock wave before the projectile. However, in the supersonic and hypersonic flow fields, a shear layer is formed which begins from the head of the projectile and extends outward from the side of the projectile. Then a multi-layer shock wave is formed composed of coronal shock waves, bottom shock waves, reflected shock waves, and Mach disk.

Key words: muzzle flow field; different velocities; dynamic mesh; two-dimensional axisymmetric

CLC number: O355 **Document code**: A **Article ID**: 1005-1120(2019)01-0088-10

0 Introduction

In recent years, there is an increasing interest in barrel firing engineering including the interior ballistic process, the intermediate ballistic process and the exterior ballistic process. During the intermediate ballistic process, the unsteady flow field with strong shock is a phenomenon with important practical significance, which affects seriously the muzzle flow field performance, and has a strong impact discontinuity and severe chemical reaction[1-3]. Shock waves propagate to the surroundings, and the intensity and propagation velocity of the shock wave are related to the relative transient pressure difference between the gas in the cannon tube and the surrounding gas[4]. The jet flow will have an impact on the firing accuracy of the projectile and will have a devastating effect on the text equipment around. There are many factors that affect the characteristics of the muzzle flow field, such as different muzzle pressures and velocities caused by the different propellant charges[5-6]. Such a flow disturbance of the large-caliber counter-mass propelling gun is quite complicated, including multiphase turbulent combustion and unsteady non-linear problems. It is difficult to obtain the accurate results of the muzzle blast wave flow rules through experiments[7-8]. Therefore, the system would be particularly important in intermediate ballistic which is known as the after-effect period[9-10].

Some mathematical representations have been developed for this complex and transient flow field, and the recent advances in computational fluid dynamics techniques become a highly effective alternative[11]. Merlen et al.[12] showed a similar rule in muzzle flow fields by the experimental study, and described a theoretical analysis in detail. Wang et al.[13] studied the whole process of 44 mm-caliber

*Corresponding author, E-mail: wanghao@mail.njust.edu.cn.

How to cite this article: LI Zijie, WANG Hao. Influence of Different Velocities on Muzzle Flow Field[J]. Transactions of Nanjing University of Aeronautics and Astronautics, 2019,36(1):88-97.
http://dx.doi.org/10.16356/j.1005-1120.2019.01.008

projectile from inside to outside based on ALE equations and dynamic grid technology. A numerical simulation of the 122 mm vehicle artillery flow field completed by Jiang et al. [14] indicated the flow phenomenon of 713 m/s projectile firing in detail. The three-dimensional unsteady chemical reaction control equations were used to simulate the 7.62 mm-caliber 735 m/s projectile with the muzzle brake by Dai et al. [15]. They described the role of the projectile and the flow field to understand the structure and ability of the muzzle flow field development process. Wang et al.[16] studied the disturbance caused by the projectile movement. It is found that the second-order TVD scheme can improve calculation accuracy of the muzzle shock wave field. Gao et al. [17] proposed the MUSCL array differential to analyze the flow field, and obtained the entire flow field image composed of air shock wave and jet structure. Florio[18] used the Osher scheme and the unstructured grid to study the behavior of a certain type cannon flow field, combining with two-dimensional or three-dimensional Euler equations. The regional grid method and the fortified solution algorithm (FSA) were used to numerically simulate the flow field caused by the movement of the projectile through the front shock wave. Based on the three-dimensional Euler equation, combined with Roe format and structural dynamic mesh technology, Zhang et al.[19] simulated the muzzle flow field with a diameter of 20 mm.

In this paper, an accurate prediction of muzzle blast waves is critical to ensure that the muzzle devices are economically viable and capable of withstanding stronger shocks. By analyzing three different muzzle velocities, computational models can help in the simulation of muzzle flow field, while limiting expensive onsite testing. Aiming at the jet structure of 300 mm-caliber, a two-dimensional axisymmetric numerical simulation model is established to study and compare the different phenomenon and parameters of the flow field and the jet structure of different velocities from inside to outside the muzzle.

1 Numerical Model

1.1 Basic assumptions

For the current study, the assumptions are as follows[20]:

(1) The gas flow is considered to be axisymmetric.

(2) Powder particles are completely burned, and the phenomenon that the powder particles are ejected out of the chamber is neglected.

(3) It is assigned as ideal gas in the flow field to satisfy the ideal gas state equation.

(4) The heat exchange between the tube and the projectile and the influence of physical strength are ignored.

1.2 Governing equations

Ignoring the effects of multicomponent and chemical reactions, the two-dimensional axisymmetric Navier-stokes equations are as follows[21-22]

$$\frac{\partial}{\partial t}\int_{\Omega(t)} \boldsymbol{Q}\mathrm{d}\Omega + \int_{\Gamma(t)} F\mathrm{d}\Gamma + \int_{\Gamma(t)} \boldsymbol{G}\mathrm{d}\Gamma + \frac{v}{y}\int_{\Omega(t)} \boldsymbol{S}\mathrm{d}\Omega = \int_{\Omega(t)} \boldsymbol{W}\,\mathrm{d}\Omega \tag{1}$$

where

$$\boldsymbol{Q} = \begin{bmatrix} \rho \\ \rho u \\ \rho v \\ \rho e \end{bmatrix}, \boldsymbol{S} = \begin{bmatrix} \rho \\ \rho u \\ \rho v \\ \rho e + p \end{bmatrix}, \boldsymbol{W} = \begin{bmatrix} 0 \\ 0 \\ 0 \\ q \end{bmatrix} \tag{2}$$

$$\boldsymbol{F} = \boldsymbol{F}_c - \boldsymbol{F}_v = \begin{bmatrix} \rho(u-u_w) - D\dfrac{\partial \rho}{\partial x} \\ \rho u^2 - \rho u u_w + p - \tau_{xx} \\ \rho u v - \rho u_w v - \tau_{xy} \\ (\rho e + p)(u-u_w) - (u-u_w)\tau_{xx} \\ -(v-v_w)\tau_{xy} + q_x \end{bmatrix} \tag{3}$$

$$\boldsymbol{G} = \boldsymbol{G}_c - \boldsymbol{G}_v = \begin{bmatrix} \rho(v-v_w) - D\dfrac{\partial \rho}{\partial y} \\ \rho u(v-v_w) - \tau_{xy} \\ \rho v(v-v_w) + p - \tau_{yy} \\ (\rho e + p)(v-v_w) - (u-u_w)\tau_{xy} \\ -(v-v_w)\tau_{yy} + q_y \end{bmatrix} \tag{4}$$

where τ_{xx}, τ_{yy}, τ_{xy}, and τ_{yx} are the viscous forces of

different direction, respectively, and shown as

$$\begin{cases}\tau_{xx}=\dfrac{2}{3}\mu\left(2\dfrac{\partial u}{\partial x}-\dfrac{\partial v}{\partial y}-\dfrac{v}{y}\right)\\ \tau_{yy}=\dfrac{2}{3}\mu\left(2\dfrac{\partial v}{\partial y}-\dfrac{\partial u}{\partial x}-\dfrac{v}{y}\right)\\ \tau_{xy}=\tau_{yx}=\mu\left(\dfrac{\partial u}{\partial y}+\dfrac{\partial v}{\partial x}\right)\end{cases} \tag{5}$$

where μ is the laminar viscous coefficient. The pressure is given by the ideal gas equation

$$p=(\gamma-1)\left[\rho e-\frac{\rho}{2}(u^2+v^2)\right] \tag{6}$$

where ρ is the gas density, u and v are the velocity components of fluids, respectively, and e is the total energy and expressed as

$$e=\frac{p}{\gamma-1}+\frac{1}{2}\rho(u^2+v^2) \tag{7}$$

where γ is gas specific heat ratio. The ideal gas state equation is $p=\rho RT$, and R is universal gas constant. q_x and q_y are the volumetric heating rate in the unit mass, respectively, which are expressed as

$$q_x=k\frac{\partial T}{\partial x}+Dh\frac{\partial \rho}{\partial x} \tag{8}$$

$$q_y=k\frac{\partial T}{\partial y}+Dh\frac{\partial \rho}{\partial y} \tag{9}$$

The type of flow is decided by σ. When $\sigma=1$, it is regarded as the two-dimensional axisymmetric model, and when $\sigma=0$, it is regarded as the two-dimensional model.

1.3 Turbulence model

This paper used the realizable k-ε turbulence model. The model has two main differences from the standard k-ε model: (1) The realizable k-ε model adds a formula for turbulent viscosity; (2) Add a new transfer equation for the dissipation rate.

Introducing the linear eddy viscosity assumption of Boussinesq, the Reynolds stress is expressed as

$$\tau_{ij}^{R}=-\overline{\rho u_i' u_j'}=\mu_t\left(\frac{\partial \boldsymbol{U}_i}{\partial x_j}+\frac{\partial \boldsymbol{U}_j}{\partial x_i}-\frac{2}{3}\frac{\partial \boldsymbol{U}_i}{\partial x_i}\right)-\frac{2}{3}\rho k\delta_{ij} \tag{10}$$

Different eddy viscosity models have different eddy viscosity coefficients. In the k-ε model, we have

$$\mu_t=f\left(\frac{\rho k^2}{\varepsilon}\right) \tag{11}$$

where

$$k=\frac{\overline{u_i' u_j'}}{2} \tag{12}$$

$$\varepsilon=v\overline{\frac{\partial u_i'}{\partial x_j}\left(\frac{\partial u_i'}{\partial x_j}+\frac{\partial u_j'}{\partial x_i}\right)} \tag{13}$$

The Schwarz inequality of Reynolds shear stress is

$$\left(\overline{u_i' u_j'}\right)^2\leqslant\overline{u_i^2 u_j^2} \tag{14}$$

2 Dynamic Mesh and Calculation Model

2.1 Boundary conditions and mesh generation

In order to simulate the motion of the projectile, considering that the projectile moves only in the X-axis direction, it is necessary to adopt the grid "layering" technique and set the overflow factor and the collapse factor. Layers of the grid are destroyed at the far end of the domain and added at the closed end of the tube to maintain the extent of the domain during the simulation. In this example, they are set as $h_i=5$ mm, $c_s=0.4$, $c_i=0.1$.

As shown in Fig.1(a), the whole computational domain is divided into three regions: Behind the projectile domain Ⅰ, in front of the projectile domain Ⅱ, and around the muzzle domain Ⅲ. In the initial state, it is 100 mm from the chamber bottom to the muzzle, and the length and width of the exterior flow field are 13 m and 3 m. The total length of the chamber tube is 29.6 m, and the tube thickness is 50 mm. The initial symmetric mesh model is shown in Fig.1(b). The minimum grid size of the two-dimensional axisymmetric model is 2 mm, and 280 000 grids in total. The computational domain is divided by structural meshes, and the interface method is used for the data interpolation calculation.

In the computational domain, the pressure-outlet boundary condition is specified as the domain boundary around the muzzle flow field. C programming languages have been created based on user-defined function (UDF) subroutines. The bottom of the cannon tube is specified as the pressure-inlet boundary condition, which is obtained through the after-effect period UDF program. The interior ballistic program written as UDF and the six-DOF pro-

gram are uploaded to control the projectile in the period of moving in the tube and out of the chamber, respectively. At all solid-fluid interfaces, insulated no-slip boundary conditions are applied.

The cannon tube is applied to the solid wall boundary condition, and the symmetry boundary condition is specified at the axis of the symmetry. At all domain boundaries, impermeable walls and temperatures near walls are applied. The initial pressure and temperature around the muzzle flow field are set as 101 325 Pa and 300 K.

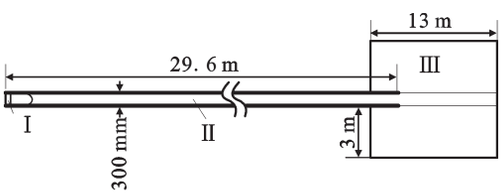

(a) Physical simulation model of 300 mm counter-mass propelling gun

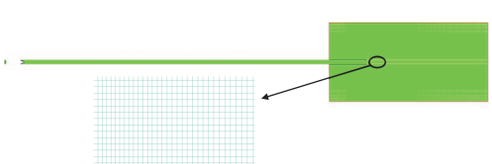

(b) Initial grid simulation model of 300 mm counter-mass propelling gun

Fig. 1 Whole computational domain and initial symmetric mesh model

2.2 Grid convergence test

Several uniform meshes have been utilized and the pressure of projectile-bottom is chosen as the grid independence demonstrating. As shown in Fig. 2, p_1, p_2 represent the pressure with the total mesh of 280 000 and 340 000, respectively. When the simulation results of two meshes become tiny,

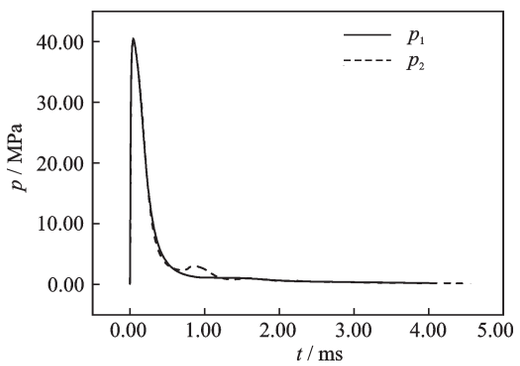

Fig.2 Pressure-time curve of projectile-bottom

the results are considered to be convergent. Our tests indicate that the grid convergence can be reached with the total meshes of 280 000 and 340 000.

2.3 Calculation model

The 300 mm-caliber counter-mass propelling gun is numerically studied in this article. The projectile and balanced body mass are 160 and 2 000 kg, respectively. Figs. 3 (a), (b) display the pressure-time and velocity-time curves of the interior ballistic accurately. Fig. 3(c) shows the after-effect period pressure-time curves. The subscripts 1, 2, and 3 represent the parameters of the velocity of 1 730.4, 978.3, and 323.4 m/s. The specific data of the muzzle pressure and muzzle velocity are shown in Table 1[23-24].

According to the Luhowski empirical formula of the after-effect period, the relationships between the muzzle pressure and the time for this example are as follows, the after-effect period of hypersonic projectile is expressed as

$$p=46.3\times10^{6}\mathrm{e}^{-24.886t} \tag{15}$$

Similarly, the expressions of supersonic and subsonic projectile are[25-26]

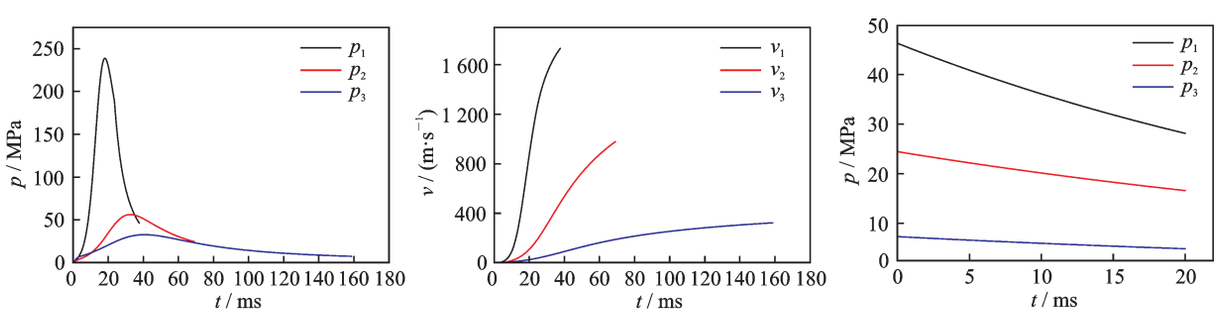

(a) Pressure-time of interior ballistic (b) Velocity-time of interior ballistic (c) Pressure-time of after-effect period

Fig.3 Comparisons of pressure and velocity in the interior ballistic and after-effect period

$$p=24.44\times10^{6}e^{-19.368t} \quad (16)$$

$$p=7.30\times10^{6}e^{-20.23t} \quad (17)$$

Table 1 Simulation results of interior ballistic

Case	Sonic velocity	Total time/ms	Muzzle velocity/(m·s^{-1})	Muzzle pressure/MPa
1	Hypersonic	37.6	1730.4	46.3
2	Supersonic	69.0	978.3	24.4
3	Subsonic	158.7	323.4	7.3

3 Analysis and Comparison

3.1 Numerical verification

In this paper, the holistic movement of a partitioned mesh processing method and realizable k-ε turbulence model are used coupling the process of the interior ballistic. Fig.4 and Fig.5 give some investigation results which represent some references of the flow field simulation. Moving boundary and Roe upwind scheme are used by Jiang et al.[27] to simulate the certain muzzle flow field of the 48 mm-caliber and 530 m/s gun. It can be seen that the blast wave system formed in Ref.[27] is consistent with this paper, which proves the reliability of this numerical method.

3.2 Comparison of initial flow field

The comparison of Mach number at the velocity of 1 730.4, 978.3, and 323.4 m/s are shown in Fig.6. Figs.7(a)—(c) show a fully developed pressure contours in the cases of three velocities. The formation and development of the initial flow field are described clearly. The projectile moves at the high velocity in the tube, continuously compresses and pushes the air before the projectile, thus form-

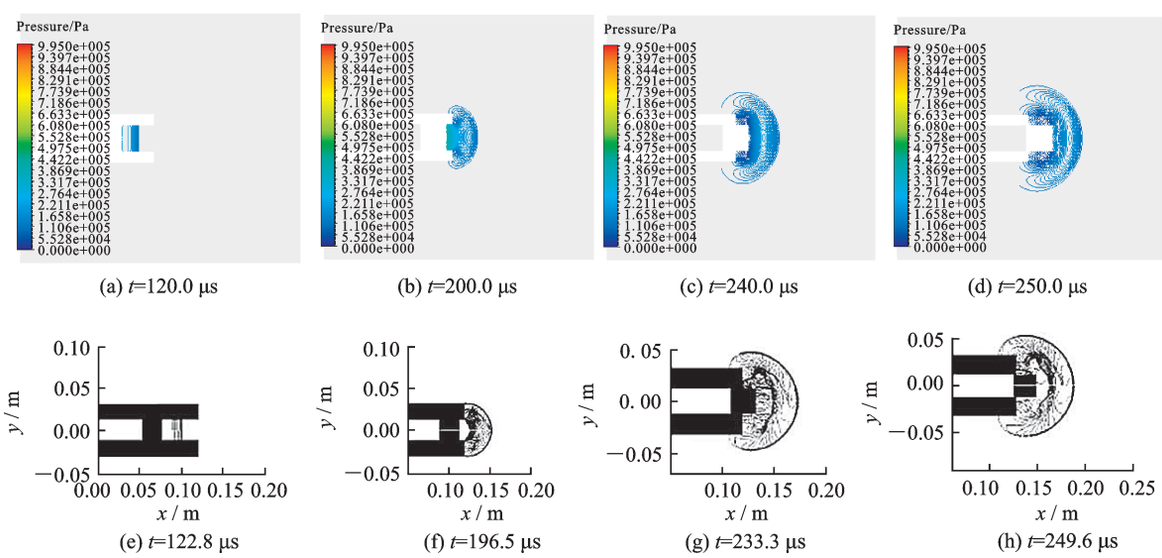

Fig.4 Comparison of pressure contours for numerical verification

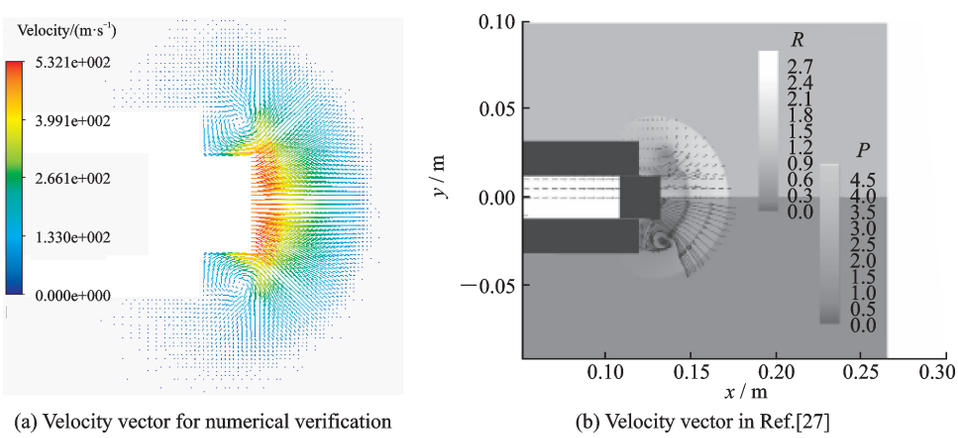

Fig.5 Comparison of velocity vectors for numerical verification

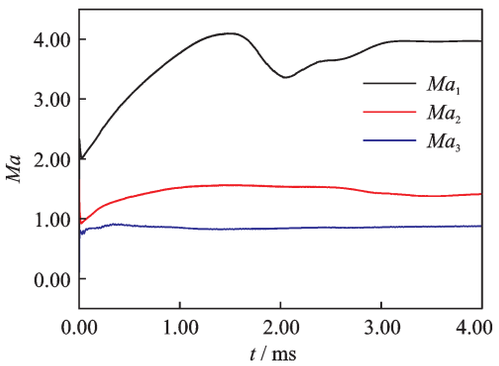

Fig.6 Mach number-time curve

ing the initial flow field.

As shown in Fig.7(a), the initial flow field is completely generated at the velocity of 323.4 m/s (0.9*Ma*), but the initial shock wave surface, the initial impact bottle and the initial Mach disk are not found. The highest pressure is just 0.11 MPa. It is ineresting to note that the disturbance of initial flow field of the subsonic projectile extends the whole computational domain. This is because the disturbance source has felt the disturbance before it arrives, meanwhile changing the flow direction and parameters to meet the disturbance source requirements. However, in the case of the supersonic and hypersonic flow field, the disturbance does not spread to the upstream disturbance source. It will not feel any disturbance before the airflow spreads here.

For the initial flow field of supersonic and hypersonic projectiles, a series of compression waves are produced when the projectile pushes the gas to spread towards the muzzle continually. With the acceleration of the projectile, the air before the projectile is squeezed out of the muzzle and propagates in the surroundings, thereby forming the initial flow field clearly.

As shown in Fig.7(b), the highest pressure in the muzzle flow field is about 0.17 MPa in the case at the velocity of 978.3 m/s (1.56*Ma*), but 0.41 MPa at the velocity of 1 730.4 m/s (4.03*Ma*) in Fig.7(c). This indicates that the intensity of the initial flow field depends mainly on the velocity of the projectile, so the higher velocity of the projectile is, the stronger blast wave ahead of projectile and the initial flow field is. As shown in Figs.7(b),(c),

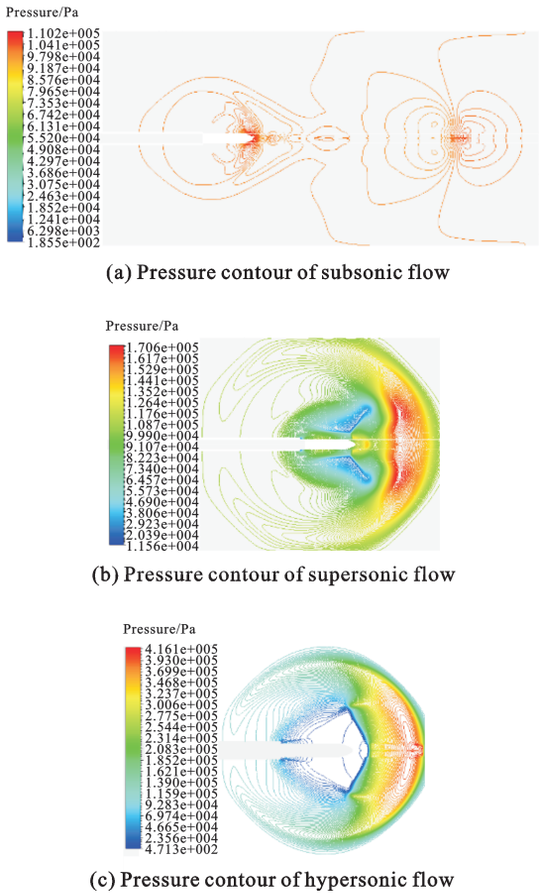

Fig.7 Pressure contours of subsonic, supersonic and hypersonic initial flow fields

the triple point and the initial Mach disk are observed clearly. The intensity of the initial flow field at the velocity of 1 730.4 m/s projectile is stronger than that of 978.3 m/s projectile more than one to two times.

3.3 Comparison of gas flow field

The propellant gas of the high pressure and temperature is ejected from the muzzle, thus creating a blast flow when the projectile is driven out of the tube absolutely. A series of compression waves are formed and spread towards the muzzle direction, mainly composed of the initial blast wave, contact surface, Mach disk, etc. The blast wave structure of the propellant gas flow at the velocitiy of 323.4, 978.3, 1 730.4 m/s, respectively are displayed in Figs.8—10.

It can be seen obviously that there are significant differences between the three gas flow field types. As shown in Fig.8, when the projectile is at the subsonic velocity, the shock wave cannot be

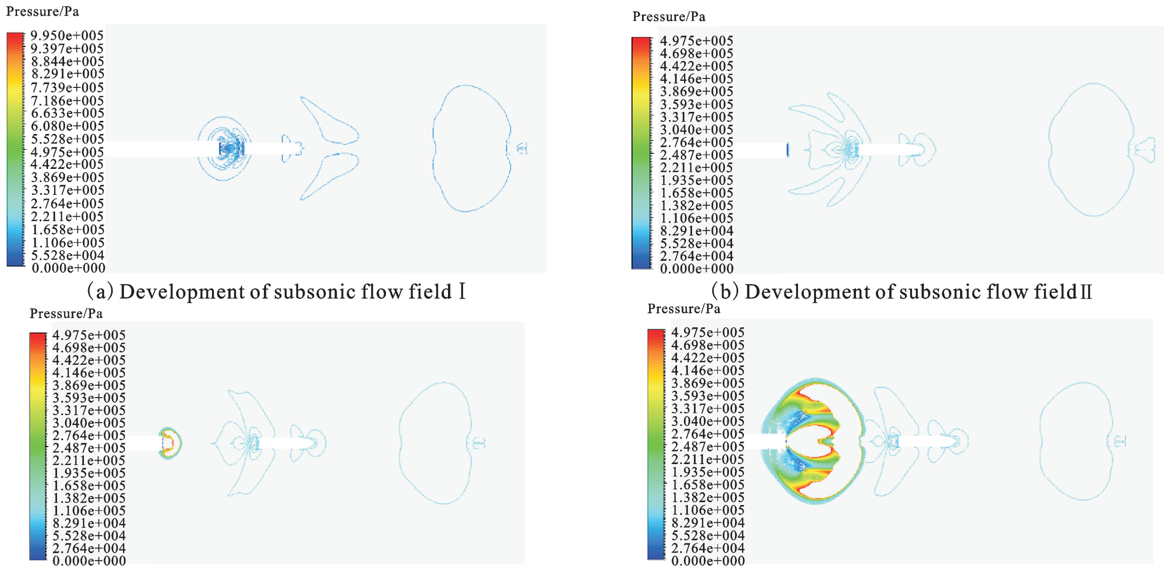

(a) Development of subsonic flow field Ⅰ (b) Development of subsonic flow field Ⅱ

(c) Development of subsonic flow field Ⅲ (d) Development of subsonic flow field Ⅳ

Fig.8 Pressure contours of subsonic gas flow field

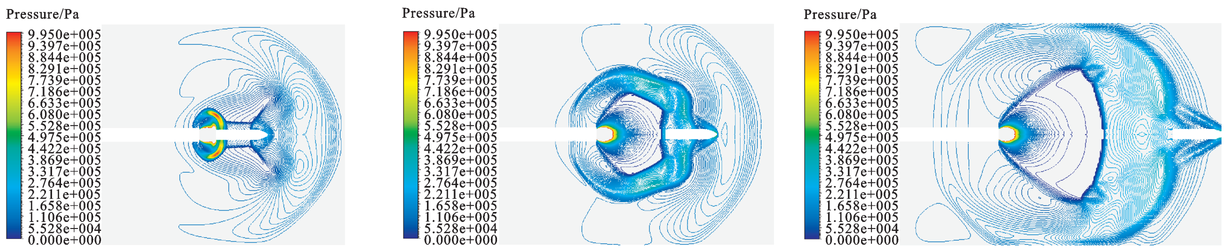

(a) Development of supersonic flow field Ⅰ (b) Development of supersonic flow field Ⅱ (c) Development of supersonic flow field Ⅲ

Fig.9 Pressure contour of supersonic gas flow field

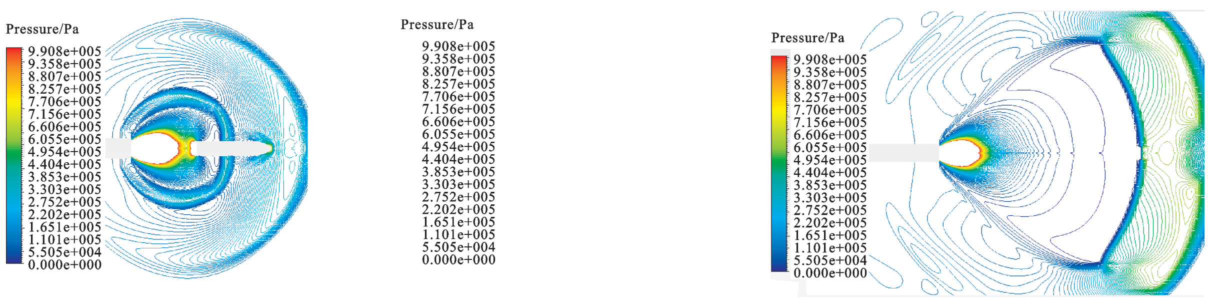

(a) Development of hypersonic flow field Ⅰ (b) Development of hypersonic flow field Ⅱ (c) Development of hypersonic flow field Ⅲ

Fig.10 Pressure contour of hypersonic gas flow field

formed clearly, as well as the propellant gas jet flow. A full wave system is also invisible, which composed of the multiple layers of shock waves, including coronary blast waves, shock waves, reflected shock waves, Mach disk and discontinuity surfaces. The shock wave at the head of projectile is as circular but it is not generated a shear layer which begins from the head of the projectile and extends outward from the side of the projectile. The shock wave at the projectile bottom has been formed following the projectile moving forward, and pressure surges can be transmitted from the rear flow field to the front. But this phenomenon cannot occur in the case of the supersonic and hypersonic flow fields.

But as shown in Fig. 9 and Fig. 10, the shock wave can be observed clearly of the supersonic and hypersonic gas flow field. As shown in Fig. 9(b), the supersonic propellant gas chases and surrounds

the projectile, the shock wave of the projectile bottom is formed clearly because the propellant gas velocity is higher than that of the projectile, which further strengthens and hinders the formation of the Mach disk. As the impact of the shock wave at the bottom of the projectile becomes weaker, the Mach disk gradually increases. At the meantime, cylindrical shock wave expands continually and blast wave spreads and decays to the distance. As a result, it is formed a whole wave system including the coronary shock wave, projectile bottom shock wave, Mach disk, etc.

As shown in Fig.10, the hypersonic propellant gas cannot chase and surround the projectile, but the shock wave of the projectile bottom is formed clearly because the propellant gas velocity is higher than the projectile velocity, which further strengthens and hinders the formation of Mach disk. Mach disk increases gradually along with the effect of shock wave of the projectile-bottom getting weaker. At the meantime, the cylindrical shock wave expands continually and blast wave spreads and decays to the distance. As a result, it is formed a whole wave system including coronary shock wave, projectile bottom shock wave, Mach disk, etc.

The velocity vectors of the supersonic and the hypersonic flow field at a same state (x=400 mm) approximately are displayed in Fig.11. It shows that the disturbance range of the supersonic flow is wider than that of the hypersonic flow.

At the subsonic, supersonic and hypersonic velocities, the parameters of the gas flow field vary widely. To achieve that purpose, two points are monitored to compare the pressure changing (Fig.12). The indices 1, 2, 3 represent the pressure of the hypersonic, supersonic and subsonic flow fields, respectively. The coordinate of the monitoring point 1 is (1 000 mm, 150 mm), and (2 000 mm, 150 mm) for point 2. The center point of the muzzle is as the origin of coordinate, the center line of the muzzle is as X-axis. The trends of the pressure are not regular. This is because the sphere of influence and the structure for three velocities are different. But the disturbance of the hypersonic is stronger than that of the other two conditions, while the disturbance at the subsonic velocity is tiny and weak.

4 Conclusions

For the 300 mm-caliber counter-mass propelling gun, we discussed the muzzle flow fields at the velocities of 323.4, 978.3 and 1 730.4 m/s, respectively. A reasonable simulation model is established coupled with the interior ballistic program and the after-effect period program. The main conclusions are as follows:

(1) The disturbance of subsonic projectiles spreads all over the computational domain. The shock wave surface, shock bottle and Mach disk are not formed, and the shock wave at the head of projectile is as circular, but it does not generate a shear layer which begins from the head of projectile and extends outward from the side of the projectile.

(2) For supersonic and hypersonic projectiles,

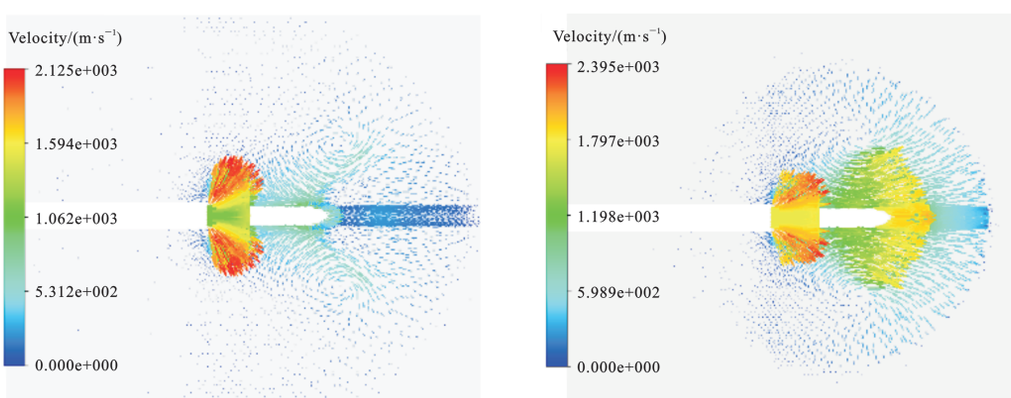

(a) Velocity vector of supersonic flow field at the same distance

(b) Velocity vector of hypersonic flow field at the same distance

Fig.11 Comparison of velocity vectors in the cases of supersonic and hypersonic

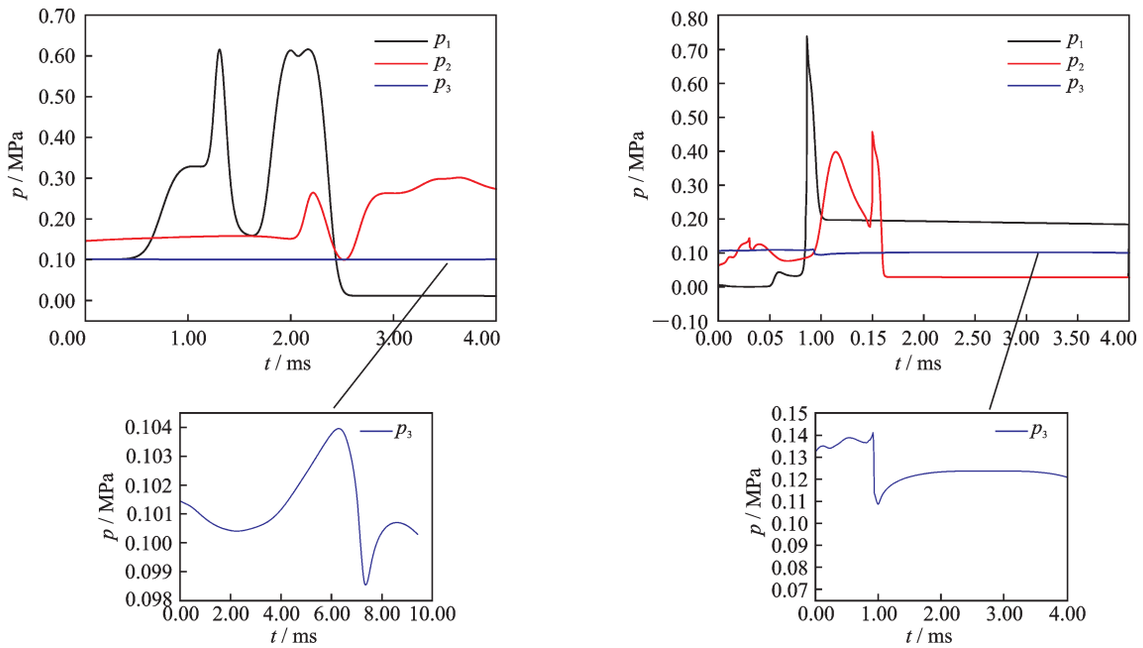

(a) Comparison of pressure for point 1 (b) Comparison of pressure for point 2

Fig.12 Comparison of pressure for two monitoring points

the shock wave of the projectile bottom is formed clearly because the propellant gas velocity is higher than that of the projectile, which further strengthens and hinders the formation of the Mach disk. It forms a whole wave system including the coronary shock wave, projectile bottom shock wave, Mach disk, etc.

(3) The strength of the initial flow field at the hypersonic velocity is the strongest and has a serious impact on the gas flow field. The initial flow field at the velocity of 1 730.4 m / s projectile is stronger than 978.3 m / s projectile more than one to two times.

References

[1] WANG L, CHEN H H, HE X. Modal frequency characteristics of axially moving beam with supersonic/hypersonic speed [J]. Transactions of Nanjing University of Aeronautics & Astronautics, 2011, 28(2): 163-168.

[2] JIANG X H, CHEN Z H, FAN B C, et al. Numerical simulation of blast flow fields induced by a high-speed projectile [J]. Shock Waves, 2008(18): 205-212. (in Chinese)

[3] WANG Y W, HUANG C G, FANG X, et al. Cloud cavitating flow over a submerged axisymmetric projectile and comparison between two-dimensional RANS and three-dimensional large-eddy simulation methods [J]. Journal of Fluids Engineering, 2016, 138(6): 1246-1256. (in Chinese)

[4] SU X P, QIAN L F, DAI J S. Muzzle flow field simulation of gun with a muzzle attachment [J]. Computer Simulation, 2009, 26(9): 15-18. (in Chinese)

[5] SUN D C, CAI T M. Effecting parameters of supersonic flow field with secondary injection [J]. Journal of Propulsion Technology, 2001, 22(2): 147-150. (in Chinese)

[6] LIU X, LIN Z X, WAN C. Simulation study of supersonic flow instability mechanism [J]. Chinese Journal of Theoretical and Applied Mechanics, 2008, 40(5): 577-584. (in Chinese)

[7] TAN L B, HOU B L, CHEN W M. Gun recoil force reduction technology [J]. Journal of Gun Launch & Control, 2006(4): 69-72. (in Chinese)

[8] VIRE A, SPINNEKEN J, PIGGOTT M D, et al. Application of the immersed-body method to simulate wave-structure interactions [J]. European Journal of Mechanics B/Fluids, 2016(55): 330-339.

[9] YOU G Z, XU H Q, YANG Q R. Intermediate Ballistic [M]. Beijing: National Defence Industry Press, 2003:1-3. (in Chinese)

[10] HE F, XIE J S, HAO P F, et al. Computation of axisymmetric jet flow with Spalart-Allmaras turbulence model [J]. Journal of Propulsion Technology, 2001, 22(1): 43-46. (in Chinese)

[11] WATANABE R, FUJII K, HIGASHINO F. Three-dimensional flow computation around a projec-

tile overtaking a preceding shock wave [J]. Journal of Spacecraft and Rockets, 1998, 35(5):619-625.
[12] MERLEN A, DYMENT A. Similarity and asymptotic analysis for gun-firing aerodynamics [J]. Journal of Fluid Mechanics, 1991, 225(225): 497-528.
[13] WANG Y, JIANG X H, Yang X P, et al. Numerical simulation on jet noise induced by complex flows discharging from small caliber muzzle [J]. Explosion and Shock Waves, 2014, 34(4): 508-512. (in Chinese)
[14] JIANG K, WANG H. Numerical simulation of muzzle flow field based on dynamic meshing technique [J]. Journal of Gun Launch & Control, 2010(3): 1-4. (in Chinese)
[15] DAI S L, XU H Q, SUN L. Numerical simulation of gun muzzle flow field including movable boundary [J]. Journal of Ballistics, 2009, 21(4): 84-87. (in Chinese)
[16] WANG S S, ZHENG J, JIA C Z, et al. Numerical simulation of muzzle blast flow field with muzzle brake [J]. Fire Control & Command Control, 2011, 36(2): 148-151. (in Chinese)
[17] GAO S Z, ZHAO R X, MA D W. Cannon computational fluid dynamics[M]. Beijing: Weapons Industry Press, 1995: 165-172.
[18] FLORIO L A. Effect of vent opening area and arrangement on gas flow field as gas propelled cylinder exits a flow tube [J]. Mechanic, 2009, 45(4): 475-501.
[19] ZHANG H H, CHEN Z H, JIANG X H, et al. Investigations on the exterior flow field and the efficiency of the muzzle brake [J]. Journal of Mechanical Science and Technology, 2013, 27(2): 95-101.
[20] ZHANG H H, CHEN Z H, JIANG X H, et al. Investigation on the blast wave structures of a high-speed projectile flying through different muzzle brakes [J]. Acta Armamentarii, 2012, 33(5): 563-567. (in Chinese)
[21] LIU X, LIN Z X, WAN C. Simulation study of supersonic flow instability mechanism [J]. Chinese Journal of Theoretical and Applied Mechanics, 2008, 40(5): 577-584. (in Chinese)
[22] ZHANG H, TAN J J, CUI D M. Numerical simulation method of flow field with muzzle attachments [J]. Journal of Gun Launch & Control, 2007(2): 48-51. (in Chinese)
[23] WENG C S, WANG H. Computing interior ballistics [M]. Beijing: National Defense Industry Press, 2006.
[24] CAI G B, WANG H Y. Numerical simulation of 3-D flow field of solid rocket motor chamber [J]. Journal of Propulsion Technology, 1995(5): 59-64.
[25] BAO T Y, QIU W J. Internal ballistics [M]. Beijing: Beijing Institute of Technology Press, 1995: 214-218.
[26] JIN Z M, WENG C S. Advanced interior ballistics [M]. Beijing: Higher Education Press, 2003. (in Chinese)
[27] JIANG X H, FAN BC, LI H Z. Numerical investigation on the muzzle flow with dynamic mesh based on ALE equation [J]. Chinese Journal of Computational Mechanics, 2008, 25(4): 563-567. (in Chinese)

Acknowledgement This work was supported in part by the National Natural Science Foundation of China (No. 51305204).

Authors Ms. **LI Zijie** is a Ph.D. student in the School of Energy and Power Engineering of Nanjing University of Science and Technology. Her research focuses on the flow field, dynamic grids and related fields.

Prof. **WANG Hao** is a doctoral supervisor in the School of Energy and Power Engineering of Nanjing University of Science and Technology. His main research areas are modern launch dynamics, aircraft ejection and control technology, and multiple reactive fluid dynamics. He is currently a senior member of the China Armed Forces Society and a member of the Academic Committee of the Key Laboratory of Special Materials Application Technology of China National Nuclear Corporation.

Author contributions Ms. **LI Zijie** designed the study, complied the models, conducted the analysis, interpreted the results and wrote the manuscript. Prof. **WANG Hao** contributed to the discussion and background of the study. All authors commented on the manuscript draft and approved the submission.

Competing interests The authors declare no competing interests.

(Production Editor: Zhang Huangqun)